AIAA JOURNAL
Vol. 35, No. 9, September 1997

Application of Chimera/Unstructured Hybrid Grids for Conjugate Heat Transfer

Kai-Hsiung Kao* and Meng-Sing Liou†
NASA Lewis Research Center, Cleveland, Ohio 44135

A method is presented that computes the conjugate heat transfer problem using a hybrid overset grid system. The hybrid grids for the fluid and solid structure regions use Chimera overset structured grids and unstructured grids, respectively. The numerical analyses require the flowfield solution and material thermal response to be obtained simultaneously. A continuous transfer of temperature and heat flux is enforced at the interface, which combines the solid structure and the fluid flow regions into an integral system. Numerical results are compared with analytical and experimental data for a flat plate and a C3X cooled turbine cascade. A simplified drum-disk system is also simulated to show the effectiveness of this hybrid grid system.

I. Introduction

PREDICTION of a turbomachinery engine's performance is a complex process entailing the iterative execution of aerodynamic, thermal, and structural analyses. In recent years, with advancements in performance of computing systems, as well as improvements in numerical schemes, computational analyses of the Navier–Stokes equations for fluid flow and heat transfer has become increasingly feasible.[1–4] Although important progress has been made in solving the Navier–Stokes equations, much work is still needed to achieve robustness, accuracy, and efficiency. An issue that concerns the efficiency and accuracy of the design analysis for engine components is the grid system used for the numerical simulation. For instance, the turbine blades are often characterized by high turning geometry and large mean flow deviation from the axial direction, resulting in substantially skewed grids. The operator power required to generate an adequate grid system for various engine components is usually expensive; the procedure is inefficient. Another issue that arises in the analysis is the thermal condition at the solid body surface. In conventional computations, the thermal conditions at the body surface are imposed with either a constant temperature condition or a prescribed heat flux condition when solving the Navier–Stokes equations. Even for industrial design processes, the wall heat transfer coefficients are often calculated using a simplified one-dimensional network flow analysis and correlations. In fact, the analysis is no longer sufficient to achieve future improvements on engine performance without considering the three-dimensional effects and the multiple physical interferences. Consequently, modifications of the one-dimensional analysis are needed in critical areas based on the information from the Navier–Stokes solutions. In reality, the temperature condition and the heat flux at the solid surface are both unknown a priori and must be determined as a part of the solution. As a result, a conjugate analysis of the fluid flow and heat transfer must be undertaken to obtain a physically realistic solution.

Among various grid systems for numerical simulation, the Chimera overset grid method[5] has been shown to have the most flexibility and efficiency in dealing with very complex configurations.[6] It consists of a set of overlapped structured grids, which are independently generated and body fitted, yielding a high-quality grid readily accessible for efficient solution schemes. Therefore, the Chimera grid method can be utilized to facilitate the grid generation process, resulting in a more efficient design procedure. Considering the conjugate problem, the fluid flow external to the solid body and the heat conduction inside the solid body must be solved in a coupled fashion. As is known in solid mechanics analysis, most structural problem can be easily resolved by using an unstructured grid method to represent a rigid body. However, depending on one type of grid method will not achieve adequate efficiency for fluid flow and solid heat transfer problems. Hence, a method that properly employs a hybrid of the Chimera and unstructured grid approaches may prove to be fruitful. A hybrid grid system using an unstructured grid to replace the arbitrarily overlapping region in the framework of the Chimera scheme, termed DRAGON grid, has been developed by Kao and Liou.[7] The original DRAGON grid method conserves the numerical fluxes at the grid interfaces and shows some promising features in terms of the solution accuracy and the grid flexibility. In this paper we adopt the approach of Ref. 7 by using the unstructured grid to resolve the heat conduction inside the solid body while remaining with the Chimera overset grid scheme for the fluid flow region.

II. Governing Equations and Numerical Algorithm

The governing equations for the fluid flow are the three-dimensional, compressible Navier–Stokes equations. The heat conduction equation is used to evaluate the temperature distributions inside a solid material.

A. Navier–Stokes Equations

The time-dependent compressible Navier–Stokes equations, expressed in integral form over an arbitrary control volume Ω, are

$$\int_{\Omega} \frac{\partial \boldsymbol{U}}{\partial t}\,\mathrm{d}v + \int_{\partial\Omega} (\boldsymbol{F} - \boldsymbol{F}_v)\cdot \mathrm{d}\boldsymbol{S} = 0 \tag{1}$$

where the conservative variable vector $\boldsymbol{U} = (\rho, \rho\boldsymbol{u}, \rho E)^T$. The inviscid flux is written as a sum of the convective and pressure fluxes: $\boldsymbol{F} = \Phi\boldsymbol{u} + \boldsymbol{P}$, where $\Phi = (\rho, \rho\boldsymbol{u}, \rho H)^T$ is the vector containing convected variables and $\boldsymbol{P} = p(0, \boldsymbol{i}, \boldsymbol{j}, \boldsymbol{k}, 0)^T$. The specific total energy is $E = H - p/\rho$. The viscous flux is $\boldsymbol{F}_v = (0, \tilde{\tau}, \tilde{\tau}\boldsymbol{u} + \boldsymbol{q})^T$. The stress tensor $\tilde{\tau}$ and the heat flux vector $\boldsymbol{q}$ are expressed in terms of gradient (∇) of relevant quantities,

$$\tilde{\tau} = -\tfrac{2}{3}\mu_v(\nabla\cdot\boldsymbol{u})\tilde{I} + \mu_v[\nabla\boldsymbol{u} + (\nabla\boldsymbol{u})^T] \tag{2}$$

$$\boldsymbol{q} = \mu_e\nabla e \tag{3}$$

where μ_v and μ_e are the transport coefficients for momentum and heat transfer, respectively. We denote the vector quantities expressed in terms of Cartesian coordinates in bold face.

1. Inviscid Fluxes

Based on the cell-centered finite volume method, the governing equations are semi-discretized. We use the new flux scheme AUSM$^+$ developed by Liou[8] to express the inviscid fluxes at the cell faces. The AUSM$^+$ scheme allows the exact capture of a normal shock by

Received Aug. 7, 1996; revision received May 16, 1997; accepted for publication May 30, 1997. This paper is declared a work of the U.S. Government and is not subject to copyright protection in the United States.

*Senior Research Associate, Institute for Computational Mechanics in Propulsion, MS 5-11, 21000 Brookpark Road.

†Senior Scientist, Turbomachinery and Propulsion System Division, MS 5-11, 21000 Brookpark Road. Associate Fellow AIAA.

using a suitably chosen interface speed of sound, yields a smoother solution by way of including higher-order polynomials, and leads to faster convergence rate.

The semidiscretized form, describing the rate of time change of $\boldsymbol{U}$ in Ω via balance of fluxes through all enclosing faces, $\boldsymbol{S}_l$, $l = 1, \ldots, LX$, whether they be in the structured or unstructured grid regions, can be cast as

$$\int_{\Omega} \frac{\partial}{\partial t}\boldsymbol{U}\,\mathrm{d}v + \sum_{l}^{LX} F_{nl}|\boldsymbol{S}_l| = 0 \tag{4}$$

where $F_{nl} = \boldsymbol{F}_l \cdot \boldsymbol{n}_l$ and $\boldsymbol{n}_l$ is the unit normal vector of $\boldsymbol{S}_l$. The task is then to represent the numerical flux at the cell interface $\boldsymbol{S}_l$, which straddles cells denoted by subscripts L and R. The AUSM$^+$ scheme gives the numerical flux in the following expression:

$$F_{nl} = \tilde{M}_l(a_l/2)(\Phi_L + \Phi_R) - |\tilde{M}_l|(a_l/2)\Delta\Phi + P_{nl} \tag{5}$$

In this formula, a_l is the speed of sound suitably defined at the interface to result in an exact resolution of a normal shock. Here $\tilde{M}_l$ is the interface Mach number. For detailed derivations and numerical evaluations of the AUSM$^+$ scheme, see Ref. 8.

2. Viscous Fluxes

For the Navier–Stokes equations, at each interface we need to define the stress tensor $\tilde{\tau}$ and the heat flux vector $\boldsymbol{q}$. The evaluation of these quantities amounts to calculating the gradients at the interfaces. This can be readily achieved by the use of the Green theorem, while maintaining consistency with the finite volume discretization. However, auxiliary cells need to be constructed with their centers located at the midpoint of the interface considered. Thus, associated with each interface, there is an auxiliary cell whose center is located at the center of the interface. The Green theorem is written as

$$\int_{v} \nabla \otimes \boldsymbol{F}_v\,\mathrm{d}v = \oint_{s} \mathrm{d}\boldsymbol{s} \otimes \boldsymbol{F}_v \tag{6}$$

where $\boldsymbol{F}_v$ is the viscous fluxes and $\otimes$ is any vector product appropriate to $\boldsymbol{F}_v$, including inner product and dyadic product, etc. As a result, the discretization of the viscous fluxes is equivalent to the central differencing in the finite difference formulation.

B. Turbulence Model

The Baldwin–Lomax[9] algebraic turbulence model is used to calculate the eddy viscosity. The effective viscosity is then given by

$$\mu = \mu_l + \mu_t = Y[(\mu_l/Pr_l) + (\mu_t/Pr_t)] \tag{7}$$

Here the subscripts l and t refer to the values in the laminar and turbulent flows. In the fluid flow and the solid body regions, the thermal conductivities remain unchanged throughout the computations. The Prandtl numbers Pr_l and Pr_t are equal to 0.71 and 0.9 for laminar and turbulent flows, respectively.

C. Heat Conduction Equation

The conductive heat transfer in the solid structure is governed by the integral heat conduction equation,

$$\int_{\Omega} \frac{\partial E}{\partial t}\,\mathrm{d}v + \int_{\partial\Omega} \boldsymbol{q} \cdot \mathrm{d}\boldsymbol{S} = 0 \tag{8}$$

where $E = \rho_s C T$ denotes the potential energy of the solid material and $\boldsymbol{q}$ is the heat flux,

$$\boldsymbol{q} = -\kappa_s \nabla T \tag{9}$$

Here κ_s is the thermal conductivity of the material, ρ_s is the density, and C is the specific heat.

The preceding integral heat equation is then expressed on each triangular cell using the finite volume method. The result is that the heat flux through a surface is calculated depending on the temperature in the neighboring cells near the surface. The change in temperature in a cell therefore can be obtained by integrating the heat fluxes throughout the surrounding cell faces. As applied in the viscous fluxes calculation, the discretization for the heat flux within the solid structure region uses central differencing formulation.

D. Time Integration

The time integration scheme updates the conservative variables at the cell centers in both fluid flow and solid heat transfer regions. The present method originates from the Taylor series expansion in time, as was done by the Lax–Wendroff scheme. Then a two-step scheme, called predictor and corrector steps, with second-order time accuracy can be obtained.

Predictor:

$$U* = U^n + \text{IBLANK} \cdot \left(\Delta t \cdot \frac{\mathrm{d}}{\mathrm{d}t}U^n\right) \tag{10}$$

Corrector:

$$U** = U* + \text{IBLANK} \cdot \left(\Delta t \cdot \frac{\mathrm{d}}{\mathrm{d}t}U*\right) \tag{11}$$

$$U^{n+1} = \frac{1}{2}(U^n + U**) = \frac{1}{2}\left\{U* + \left[U^n + \Delta t \cdot \frac{\mathrm{d}}{\mathrm{d}t}U*\right]\right\} \tag{12}$$

It is noted that 1) the predictor step allows a full time step, 2) only two levels of storage are needed as U^n is absorbed in forming the residual indicated in the square bracket, and 3) both predictor and corrector steps are identical, with no need of defining a midpoint for the corrector step, leading to simplification of coding and the complexity of evaluating the transport terms. The scheme is explicit and, therefore, conditionally stable for Courant–Friedrichs–Lewy numbers less than 1 and uses local time stepping to accelerate steady state convergence. The IBLANK values in Eqs. (10) and (11) are either 0 or 1 depending on the classification of the grid cell and will be identified in the following section.

III. Grid Methods

The Chimera composite grid method has been shown to be very flexible and efficient in generating body-fitted structured grids for complex configurations. In the solid mechanics community, unstructured grid techniques are widely used to represent structural domains. The current method adopts the benefits of both structured and unstructured grids to make conjugate heat transfer problems more accurate and simple to implement.

A. Chimera Grid

The Chimera scheme[5,10,11] is a grid embedding technique that provides a conceptually simple method for domain decomposition. For instance, a major grid, is generated about a main body element and minor grids are then overset on the major grid so as to resolve interesting features of the configuration. Usually the minor grids are overset on top of the major grid without requiring the mesh boundaries to join in any special way. However, a common overlap region is always required to provide a means of matching the solution across boundary interfaces. To increase the flexibility in the selection of subdomains, the Chimera scheme also allows for the removal of regions of a mesh containing an embedded grid. That is, an embedded mesh introduces a hole into the mesh in which it is embedded. Typically, a hole is defined by a creation boundary, which contains a surface or a group of surfaces. The purpose of a hole creation boundary is to identify points that are within this boundary. A mesh point is considered to be inside a hole creation boundary if it is inside all surfaces that define the boundary. The hole information from the Chimera grid package is stored in an array, IBLANK, which is defined for each grid cell as

$$\text{IBLANK} = \begin{cases} 1, & \text{if a point is not blanked} \\ 0, & \text{if a point is blanked} \end{cases}$$

Figure 1 illustrates the connections between composite overlapping grids, with hole points being blanked by a prescribed creation boundary. A practical application of the Chimera grid system for the complete Space Shuttle/Solid Rocket Booster geometry[6] is shown in Fig. 2 (Ref. 23).

A flow solver must be modified to account for the use of multiple meshes and the holes in the grids. These hole points must be blanked or excluded from the flowfield solution. The main change in the flow algorithm itself is the treatment of the hole boundaries. The blanked solutions are updated in the interpolation routine. With this

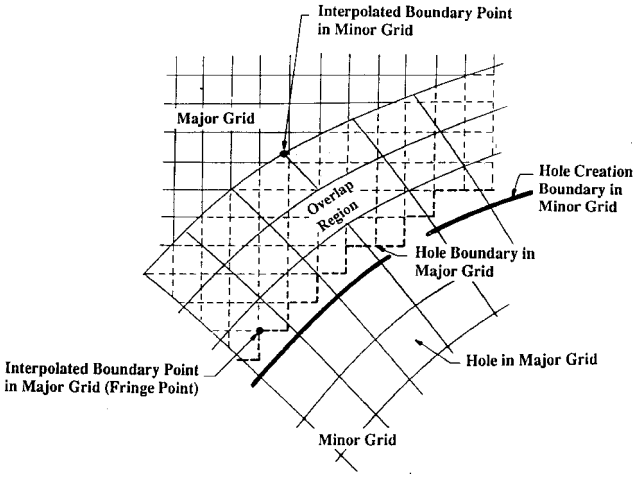

Fig. 1 Interconnections of minor and major grids for Chimera overset grid scheme.[11]

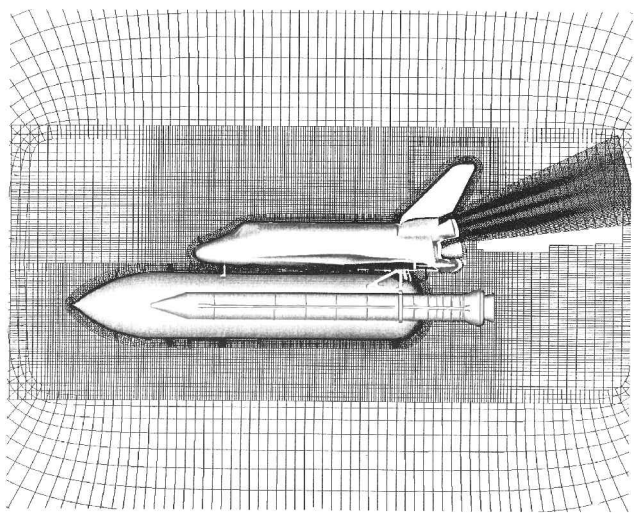

Fig. 2 Chimera grid used for integrated Space Shuttle geometry.[23]

approach, no special routine or logic tests are required to exclude the blanked points from the flowfield solution. Details regarding the grid embedding technique can be found in Refs. 10–12.

B. Unstructured Mesh

The Delaunay triangulation scheme is applied to generate an unstructured grid in the solid material region. The steps for adopting the unstructured cells in the framework of the Chimera grid scheme are summarized next.

1) Boundary nodes, which define the solid material region, are first identified from the Chimera grid composite process.

2) Boundary nodes are reordered according to their geometric coordinates.[13]

3) The Delaunay triangulation method is then performed to connect these boundary nodes and generate triangular meshes within the solid region based on the Bowyer algorithm.[14]

4) For the unstructured grid system, there is no logical ordering of the cells and their neighbors; connectivity matrices containing cell-based as well as edge-based information must be introduced. Also, the present approach requires additional matrices to connect the structured and unstructured grids. The connectivity matrices used in the present two-dimensional version are summarized as follows: a) IEDGENODE(1:2, edges), two nodes for each edge; b) ICELLEDGE(1:3, cells), three edges for each triangular cell; c) IEDGECELL(1:2, edges), two neighboring cells for each edge; d) IEDGETYPE(edges), edge type (type of boundary condition); e) IEDGEFLUX(grids, edges), edge number that connects structured and unstructured grids, where the parameter grids identifies which structured grid; f) IFLUXINDX(grids, edges), i index of the structured cell that shares the edge fluxes with the unstructured cell; and g) IFLUXINDY(grids, edges), j index of the structured cell that shares the edge fluxes with the unstructured cell.

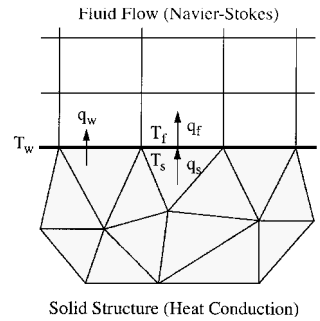

Fig. 3 Heat flux at the cell face connecting the structured and unstructured grids.

The first four types of connectivities matrices are standard in unstructured grid codes, except that we assign plus and minus values to IEDGETYPE to indicate whether the outward normal vector of a triangular cell face points into or out of the neighboring structured cell that shares the same face. This information is needed as the temperature and heat flux conditions are enforced to be identical on this face.

C. Data Communication Through Grid Interfaces

In the Chimera method, communication between overlaid grids is achieved by interpolation of boundary values from the mesh or meshes in which the boundaries are contained. We have used the PEGSUS codes[10,11] to make interconnection of subdomains, define the holed region, and supply points to facilitate communication among grids during the solution process. At present, the Chimera scheme employs trilinear interpolation, which, as some simple experiments have shown,[15–18] is superior to Taylor series expansion.

In the current work, both the structured and unstructured solver are based on the cell centered scheme in which the quadrilateral and triangular cells are used, respectively. Figure 3 shows the interfaces connecting both structured and unstructured grids. As noted, the heat flux, evaluated at the cell interface, is based on the conditions of neighboring cells. In the conjugate problem, the temperature and the heat flux values at the interface are enforced to be identical according to the following relations:

$$T_w = T_f = T_s \tag{13}$$

$$\boldsymbol{q}_w = -\kappa_f \nabla T_f = -\kappa_s \nabla T_s \tag{14}$$

Here the subscripts w, f, and s denote the values at the solid body surface, the fluid boundary, and the solid boundary, respectively. Note that the boundary interface conditions updated in Eqs. (13) and (14) are not iterated because only steady-state solutions are considered throughout the present computations.

IV. Test Results and Discussions

Numerical results are validated and compared with analytical and experimental data for a flat plate and a C3X cooled turbine cascade. The heat transfer coefficients and temperature distributions along the solid body surfaces are well predicted. A simplified drum-disk system is also simulated to show the effectiveness of the hybrid grid method. For those test cases, a dense grid is applied on regions near the solid surfaces to accurately resolve the boundary and thermal layers. Typically, the numerical solutions were obtained on the Cray Y-MP supercomputer with 3.7×10^{-5} s per grid point for each iteration. No significant effect on convergence rate to steady state has been encountered in our calculations.

A. Case 1: Conjugate Heat Transfer on a Flat Plate

The first case calculates the laminar flow past a flat plate with a cylindrical leading edge, as shown in Fig. 4. The upstream flow conditions are $M = 0.3$, $Re_l = 10^4$, $Pr = 0.71$, and $T = 300$ K. Here $l = 1$ m is the chord length of the plate, and the wall thickness is 1.5 mm. Aluminum, with a density of 2700 kg/m^3, thermal conductivity of 211 W/m-K and a specific heat of 900 W-s/kg-K, is used as the plate material. The inner wall temperature is 280 K throughout the computation.

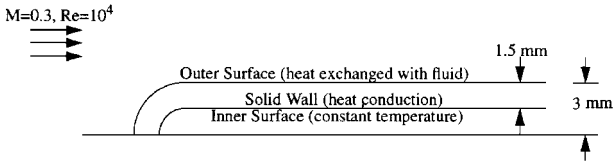

Fig. 4 Conjugate heat transfer on a semi-infinite flat plate.

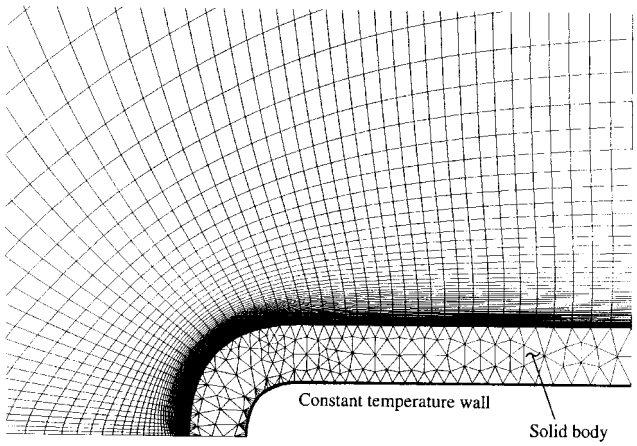

Fig. 5 Hybrid grid system for a cooled flat plate.

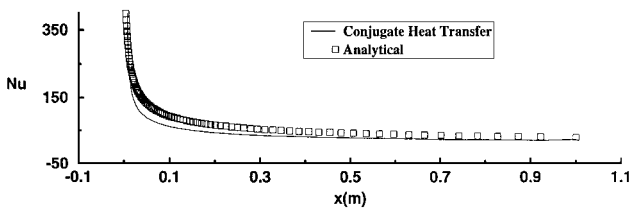

Fig. 6 Comparison of the Nusselt number between conjugated and analytical data.

Under these conditions, the temperature along the outer wall is nearly constant and equal to the inner wall temperature. Therefore, the calculated Nusselt number can be compared with the analytical values, which are given for a flat plate of zero thickness and constant wall temperature by Eckert and Weise[19]:

$$Nu = 0.333\sqrt[3]{Pr}\sqrt{Re_x}\quad (l/x) \tag{15}$$

Here x is the distance from the leading edge of the plate. The computed Nusselt number can be obtained by

$$Nu = \frac{q\quad l}{\kappa_f(T_w - T_a)} \tag{16}$$

where q is the heat flux, l is the plate length, T_w is the wall temperature, T_a is the adiabatic wall temperature, and κ_f is the thermal conductivity of the fluid.

Figure 5 shows the hybrid grid system used for the flat plate case. The external flowfield is first resolved using one structured mesh with grid dimensions of 168×50. The Delaunay triangulation method is then used to construct the unstructured grid to represent the flat plate. In this case, we use 530 nodes and 800 triangular cells for the unstructured grid region. The computed Nusselt numbers along the plate surface are compared with the analytical values and displayed in Fig. 6. The profiles are nearly identical everywhere except near the leading edge, where the analytical results are not valid.

B. Case 2: C3X Cooled Turbine Cascade

In this case, the C3X cooled turbine cascade reported by Hylton et al.[20] is simulated for the conjugate heat transfer solution. The blade geometry considered has been shown experimentally to exhibit a two-dimensional response. The blade was instrumented with surface thermocouples and pressure sensors. Data on the blade surface were acquired via a computer controlled data acquisition system, and reduced data are tabulated and reported in Ref. 20.

A C3X test case (run 112) was selected and its setup conditions are listed in Ref. 20. The coolant flow conditions and the experimentally determined external blade wall temperature, heat transfer coefficient, and pressure distributions are also described in that report.

At the inlet, for run 112, the Mach number is 0.17, the Reynolds number is 5.3×10^5, the total temperature is 783 K, and the total pressure is 6.22 kPa. The blade geometry has a high turning angle, which complicates the grid generation process. Previous grid dependency studies[3,4,21,22] for this test case suggest that a sufficient Chimera overset grid system would be an O-type grid (size 139×51) wrapping around the turbine cascade and H type (size 76×70) for the fluid flow path, as shown in Fig. 7. This grid system is easily applied, preserves high grid quality at the region near the blade body, and maintains the grid periodicity at the upper and lower boundaries. The Navier–Stokes solution was calculated with $y^+ = 0.5$ for the first node from the wall. The Delaunay triangulation method is then used to generate the unstructured grid representing the inner region of the blade, with a grid size of 610 nodes and 1001 triangular cells. Note that the 10 cooling holes, are also included to simulate the conjugate heat transfer solution with cooling effect. Also, constant temperature conditions are employed for the cooling holes, and their values are listed in Ref. 20. The solid material used for the blade body is stainless steel.

Two types of blade boundary conditions are applied in this test case: 1) adiabatic wall and 2) conjugate blade surface with internal cooling effect. Residual reductions in L_∞-norm by two orders of magnitude were used to obtain the converged heat transfer results. Figures 8 and 9 illustrate the Mach number contours and the temperature distributions for the adiabatic and conjugate cases, respectively. In Fig. 10, the pressure distributions vs the normalized distance (x/c) from the leading edge of the blade for both the adiabatic wall and conjugate wall cases indicate close agreement with the experimental data.

As the results plotted in Fig. 11 indicate the adiabatic wall temperature is significantly higher than the experimentally determined blade surface temperature. By including internal cooling, the blade

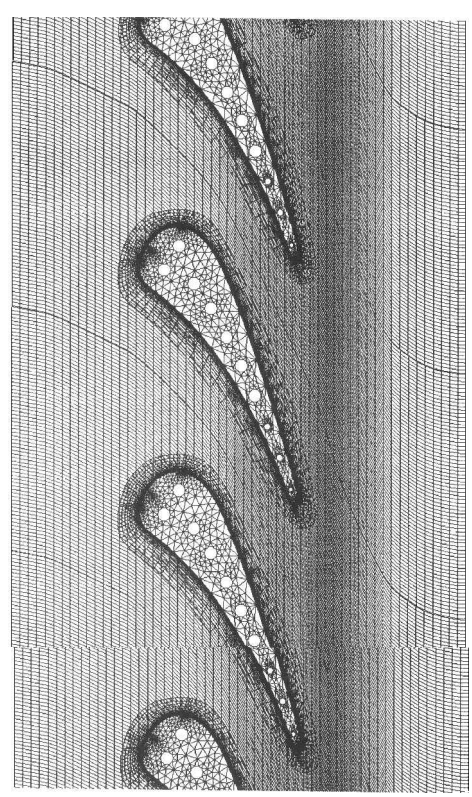

Fig. 7 Chimera/unstructured grid system used for C3X turbine cascade with 10 cooling holes.

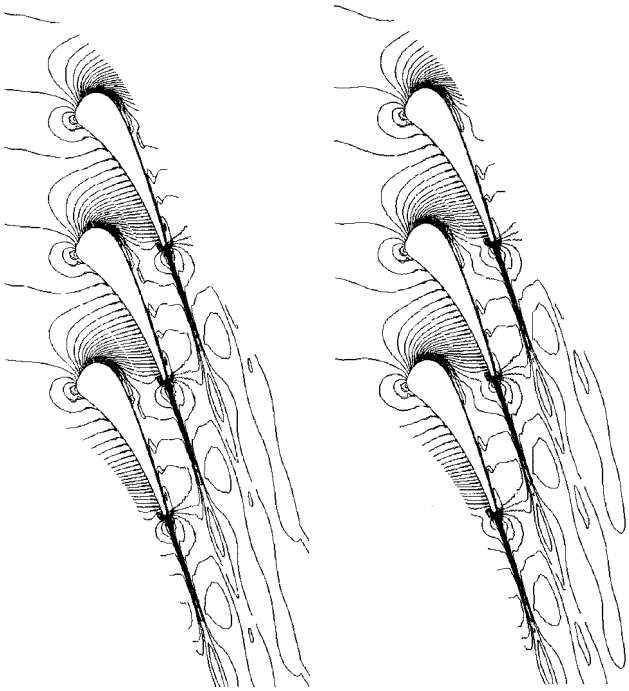

a) Adiabatic wall b) Conjugate with cooling

Fig. 8 Mach contours for C3X turbine cascade with adiabatic and conjugate walls: $M_{max} = 1.3$, $M_{min} = 0$, and $\Delta M = 0.0165$.

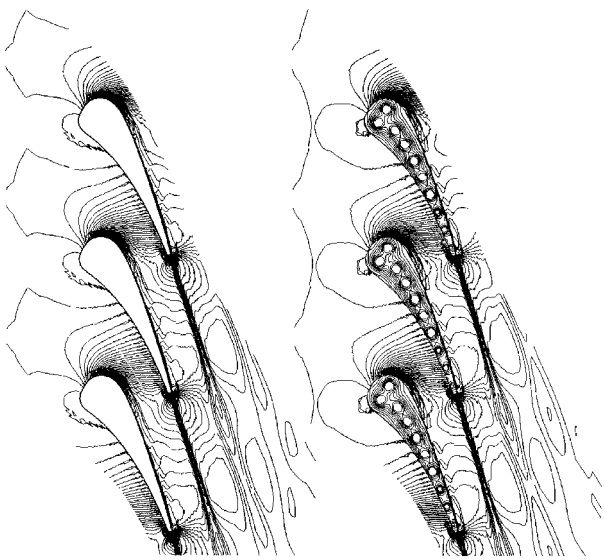

a) Adiabatic wall b) Conjugate with cooling

Fig. 9 Temperature distributions in the C3X turbine cascade flows; $T_{max} = 1.4$, $T_{min} = 0.4$, and $\Delta T = 0.003$ in fluid region and $T_{max} = 0.5$, $T_{min} = 0.4$, and $\Delta T = 0.0004$ in disk region.

temperature prediction greatly improved. It is seen that the conjugate blade temperature (shown in Fig. 11) agrees well with the experimental data in both the pressure and the suction regions. However, the discrepancy shown around the trailing edge of the blade indicates either a higher-order turbulence model or refined grid resolution may be needed to improve the solution of the wake flow.

C. Case 3: Simplified Drum-Disk System

A secondary flow system in a gas turbine engine is an example of a flow that requires aero, thermal, and structural analyses. In this test case, a simplified drum-disk flow system is simulated using the present hybrid grid method. Rotating effects of the drum-disk system are not considered in the present calculation. Inasmuch as no experimental data is available for this simulation, the results simply illustrate the versatility of the current method.

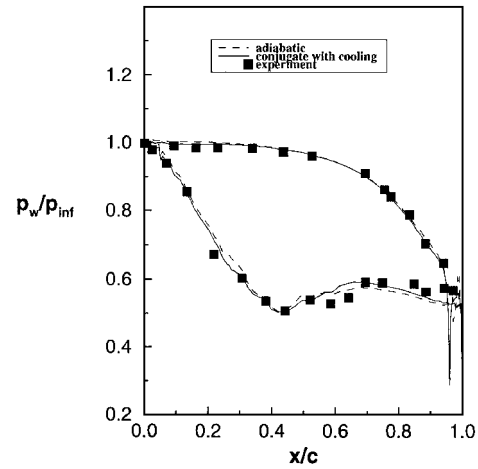

Fig. 10 Pressure distributions along the blade surface.

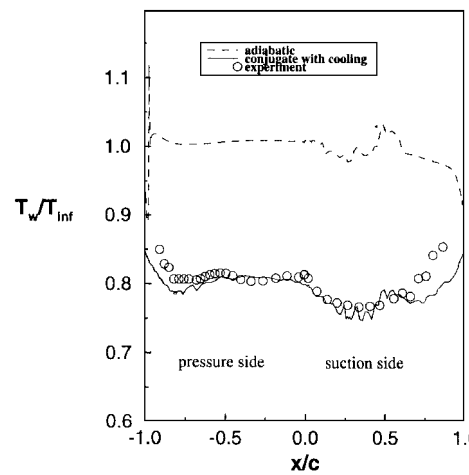

Fig. 11 Temperature distributions along the blade surface.

As shown in Fig. 12, the Chimera overset grid scheme is used to represent the interior region between the drum and the disk. It is noted that the disk grid (88×21) is embedded on the drum grid (116×61). Consequently, those grid points inside a prescribed hole creation boundary have been blanked out from the drum grid. As also shown in Fig. 12, an unstructured grid has been constructed to fill in the disk body, with a grid size of 195 nodes and 301 triangular cells.

The fluid flow with $M = 0.5$, $T = 300$ K, and $Re = 10^3$ is injected from the left entrance and leaves the drum-disk system from the right with a back pressure ratio $P_{exit}/P_{in} = 0.7$. A constant surface temperature of 280 K is used for the entire drum body except for the disk region. In this test case, two types of thermal boundary conditions are used at the disk-fluid conjugate surface, namely, the adiabatic wall and conjugate heat transfer wall conditions. Figure 13 illustrates the Mach number contours within the drum-disk cavities. The rotating motion, which causes a delicate balance between pressure, centrifugal, and buoyancy forces, is not considered in this drum-disk system. It is apparent from the plots that the effect of heat transfer has little influence on the fluid flow solution.

The computed temperature distributions for the drum-disk system are shown in Fig. 14, indicating similar contours in the fluid region except near the disk surface. Comparisons of the temperature distributions along the disk body surface are plotted in Fig. 15, showing that the average adiabatic wall temperature is much higher than the conjugate wall temperature. Subject to the adiabatic wall assumption, the heat flux is mainly convected by the fluid flow, and its value vanishes at the disk body surface, causing a large temperature deviation. With the conjugate wall condition, the heat flux is conducted as well as convected within the fluid flow and solid body regions, providing a better thermal exchange at the disk surface. Note that the temperature variations along the surface of the disk body are rather small, and this trend is consistent with the design condition in the secondary flow system (interior data for Pratt Whitney PW4000 engine).

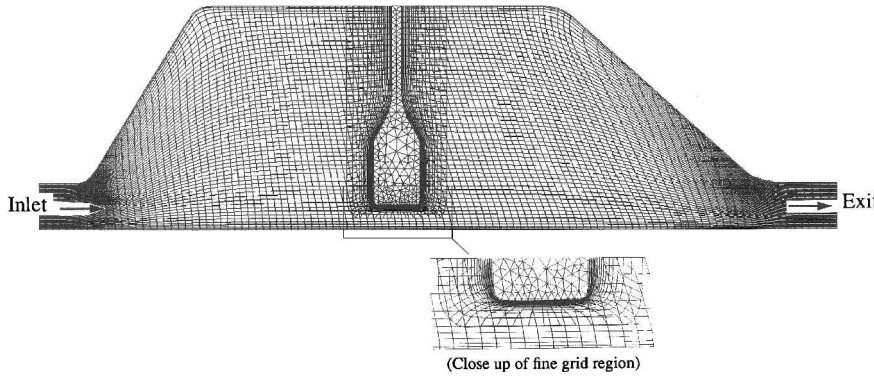

Fig. 12 Simplified drum-disk system using Chimera/unstructured grids.

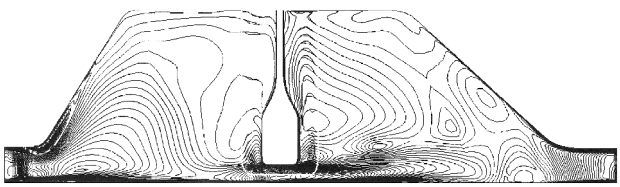

a) Adiabatic wall

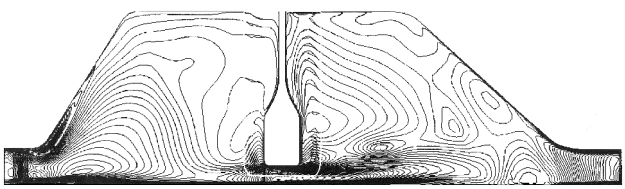

b) Conjugate wall

Fig. 13 Comparisons of Mach number contours for simplified drum-disk system; $M_{max} = 0.7$, $M_{min} = 0$, and $\Delta M = 0.03$.

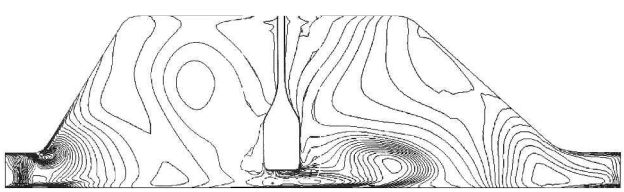

a) Adiabatic wall

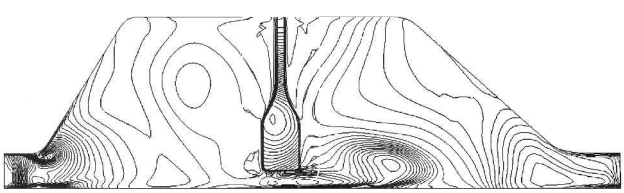

b) Conjugate wall

Fig. 14 Comparisons of the temperature contours for simplified drum-disk system; $T_{max} = 1$, $T_{min} = 0.6$, and $\Delta T = 0.01$ in fluid region and $T_{max} = 0.7$, $T_{min} = 0.6$, and $\Delta T = 0.0004$ in disk region.

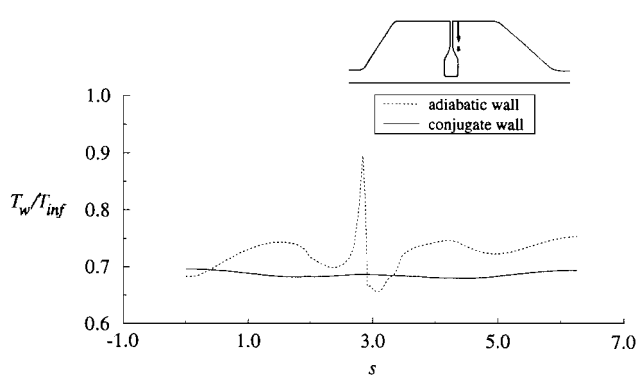

Fig. 15 Temperature distributions along the disk body surface

V. Conclusions

This paper presented a method that computes the conjugate heat transfer problem using a hybrid overset grid system. The hybrid grids for the fluid flow and solid structure regions use Chimera overset structured grids and unstructured grids, respectively. During the computational process, the method continuously transfers temperature and heat flux at the cell interfaces between the fluid and solid regions with no artificial temperature distribution or prescribed heat transfer rate. Two validation cases of a flat plate and the cooled C3X turbine cascade have been tested. For the flat plate, heat transfer rates indicate the temperature along the plate surface is well preserved involving conjugate heat transfer calculation. For the turbine case, the effects of heat conduction in the solid regions are shown to significantly affect the computed surface temperatures in comparison to those obtained from a traditional adiabatic wall assumption, indicating a conjugate calculation is essential to obtain accurate solution. A simplified drum-disk system illustrates the versatility of the current grid method. With the proposed hybrid grid system, aerodynamic analysis for designing engine components can now efficiently include aero, thermal, and structural effects as one integral system.

Acknowledgments

This work was performed under Grant NCC3-370 from the NASA Lewis Research Center; the Project Monitor is Charles Lawrence at the Computing and Interdisciplinary Systems Office. The computational results for the test problems are obtained using the Cray Y-MP computer system and partly calculated on the Cray C90 at NASA Ames Research Center.

References

[1]Chima, R. V., "Inviscid and Viscous Flows in Cascade with an Explicit Multi-Grid Algorithm," *AIAA Journal*, Vol. 23, No. 10, 1985, pp. 1556–1563.

[2]Davis, R. L., Ni, R. H., and Carter, J. E., "Cascade Viscous Flow Analysis Using the Navier–Stokes Equations," AIAA Paper 86-0033, Jan. 1986.

[3]Kwon, O. K., "Navier–Stokes Solution for Steady Two-Dimensional Transonic Cascade Flows," *Journal of Turbomachinery*, Vol. 110, 1988, pp. 339–346.

[4]Boyle, R. J., "Navier–Stokes Analysis of Turbine Blade Heat Transfer," *Journal of Turbomachinery*, Vol. 113, 1991, pp. 392–403.

[5]Benek, J. A., Buning, P. G., and Steger, J. L., "A 3-D Chimera Grid Embedding Technique," AIAA Paper 85-1523, July 1985.

[6]Buning, P. G., Chiu, I. T., Martin, F. W., Jr., Meakin, R. L., Obayashi, S., Rizk, Y. M., Steger, J. L., and Yarrow, M., "Flowfield Simulation of the Space Shuttle Vehicle in Ascent," *Proceedings of the Fourth International Conference on Supercomputing* (Santa Clara, CA), April 1989, pp. 20–28.

[7]Kao, K. H., and Liou, M. S., "Advance in Overset Grid Schemes: from Chimera to DRAGON Grids," *AIAA Journal*, Vol. 33, No. 10, 1995, pp. 1809–1815.

[8]Liou, M. S., "A Continuing Search for a Near-Perfect Numerical Flux Scheme; Part I: AUSM+," NASA TM 106524, March 1994.

[9]Baldwin, B. S., and Lomax, H., "Thin Layer Approximation and Algebraic Model for Separated Turbulent Flows," AIAA Paper 78-20776, Jan. 1978.

[10]Benek, J. A., Steger, J. L., Dougherty, F. C., and Buning, P. G., "Chimera: A Grid-Embedding Technique," Arnold Engineering Development Center, Rept. AEDC-TR-85-64, April 1986.

[11]Suhs, N. E., and Tramel, R. W., "PEGSUS 4.0 User's Manual," Calspan Corp./AEDC Operations, Rept. AEDC-TR-91-8, Nov. 1991.

[12] Steger, J. L., and Benek, J. A., "On the Use of Composite Grid Schemes in Computational Aerodynamics," *Computational Methods in Applied Mechanics and Engineering*, Vol. 64, Nos. 1–3, 1987.

[13] Barth, T. J., "Aspects of Unstructured Grids and Finite-Volume Solvers for the Euler and Navier–Stokes Equations," von Kármán Inst. for Fluid Dynamics, Lecture Series 1994-05, March 1994.

[14] Bowyer, A., "Computing Dirichlet Tessellations," *Computer Journal*, Vol. 24, No. 2, 1981, pp. 162–166.

[15] Mastin, C. W., and McConnaughey, H. V., "Computational Problems on Composite Grids," AIAA Paper 84-1611, June 1984.

[16] Meakin, R. L., "On the Spatial and Temporal Accuracy of Overset Grid Methods for Moving Body Problems," AIAA Paper 94-1925, June 1994.

[17] Parthasarathy, K. N., "Numerical Procedure for Aircraft/Store Flow Field," Quarterly Progress Repts. 4–6, NASA Contract NAS2-11742, General Dynamics, Fort Worth, TX, 1984.

[18] Part-Enander, E., and Sjogreen, B., "Conservative and Non-Conservative Interpolation Between Overlapping Grids for Finite Volume Solutions of Hyperbolic Problems," *Computers and Fluids Journal*, Vol. 23, No. 3, 1994, pp. 551–574.

[19] Eckert, E., and Weise, W., "Die temperature unbeheizter korper in einem gasstrom hoher geschwindigkeit," *Forschg. Ing.-Wes.*, Vol. 12, 1941, pp. 40–50.

[20] Hylton, L. D., Mihelc, M. S., Turner, E. R., Nealy, D. A., and York, R. F., "Analytical and Experimental Evaluation of the Heat Transfer Distribution over the Surface of Turbine Vanes," NASA CR-168015, May 1983.

[21] Hall, E. J., Topp, D. A., and Delaney, R. A., "Aerodynamic/Heat Transfer Analysis of Discrete Site Film-Cooled Turbine Airfoils," AIAA Paper 94-3070, June 1994.

[22] Barber, T. J., Choi, D., McNulty, G. S., Hall, E. J., and Delaney, R. A., "Preliminary Findings in Certification of ADPAC," AIAA Paper 94-2240, June 1994.

[23] Gomez, R. J., III, Martin, F. W., Jr., Ma, E. C., and Slotnick, J. P., "Analysis of the Space Shuttle Ascent Aerodynamic Environment," Proceedings of the AIAA 2nd Overset Composite Grid and Solution Technology Symposium, Fort Walton Beach, FL, Oct. 1994.

J. Kallinderis
Associate Editor